

Unusual Photophysical Properties of a Ruthenium(II) Complex Related to $[\text{Ru}(\text{bpy})_2(\text{dppz})]^{2+}$

Yujie Sun,[†] Sibrina N. Collins,^{*,‡} Lauren E. Joyce,[†] and Claudia Turro^{*,†}

[†]Department of Chemistry, The Ohio State University, Columbus, Ohio 43210, and

[‡]Department of Chemistry, College of Wooster, Wooster, Ohio 44691

Received December 19, 2009

A new ruthenium polypyridyl complex, $[\text{Ru}(\text{bpy})_2(\text{dpqp})]^{2+}$ (bpy = 2,2'-bipyridine; dpqp = pyrazino[2',3':5,6]pyrazino[2,3-f][1,10]phenanthroline), shows strong luminescence in water at room temperature, a behavior that is strikingly different from that of the nonemissive "DNA light-switch" prototype $[\text{Ru}(\text{bpy})_2(\text{dppz})]^{2+}$ (dppz = dipyrido[3,2-a:2'-3'-c]-phenazine) under similar conditions. Variation of the absorption and emission spectra of $[\text{Ru}(\text{bpy})_2(\text{dpqp})]^{2+}$ as a function of the pH is consistent with the occurrence of two ground-state protonation steps associated with the dpqp ligand and an apparent pK_a^* of 2.1. Electrochemistry and theoretical calculations indicate that the lowest unoccupied molecular orbital (LUMO) of $[\text{Ru}(\text{bpy})_2(\text{dpqp})]^{2+}$ is localized on the distal portion of the dpqp ligand and lies at a lower energy than the dppz-based LUMO of $[\text{Ru}(\text{bpy})_2(\text{dppz})]^{2+}$. The combination of its strong DNA binding affinity and relatively long-lived triplet metal-to-ligand charge-transfer excited state in an aqueous solution results in more efficient DNA photocleavage by $[\text{Ru}(\text{bpy})_2(\text{dpqp})]^{2+}$ than $[\text{Ru}(\text{bpy})_2(\text{dppz})]^{2+}$.

Introduction

Ruthenium polypyridyl complexes, such as $[\text{Ru}(\text{bpy})_3]^{2+}$ (**1**; bpy = 2,2'-bipyridine), are among the most investigated in fields that include solar energy conversion,^{1–3} artificial photosynthesis,^{4,5} and optical sensing,^{6–8} owing to their favorable photophysical properties, excited state reactivity, and chemical stability.^{9–11} An important complex of this type is the "DNA light-switch" molecule $[\text{Ru}(\text{bpy})_2(\text{dppz})]^{2+}$ (**2**; dppz = dipyrido[3,2-a:2'-3'-c]phenazine; Figure 1), whose negligible luminescence in water is enhanced dramatically ($> 10^6$) upon the addition of double-stranded DNA.¹²

Numerous ruthenium complexes complexed by derivatives of the dppz ligand have been explored since the first report of **2** in 1990,^{13–16} and abundant experimental and theoretical work aimed at the elucidation of the light-switch mechanism can be found in the literature.^{17–22}

Ruthenium(II) complexes with dppz ligands, such as **2**, are known to possess low-lying triplet metal-to-ligand charge-transfer (³MLCT) excited states localized on the π^* orbitals of the dppz ligand proximal (³MLCT^{prox}, bpy) and distal (³MLCT^{dis}, phenazine) to the metal center.^{23,24} The temperature dependence of the luminescence of **2** has demonstrated

*To whom correspondence should be addressed. E-mail: turro@chemistry.ohio-state.edu (C.T.), scollins@wooster.edu (S.N.C.).

- (1) Gratzel, M. *Nature* **2001**, *414*, 338.
- (2) Lewis, N. S.; Nocera, D. G. *Proc. Natl. Acad. Sci. U.S.A.* **2006**, *103*, 15729.
- (3) Huynh, M. H. V.; Dattelbaum, D. M.; Meyer, T. J. *Coord. Chem. Rev.* **2005**, *249*, 457.
- (4) Sykora, M.; Maxwell, K. A.; DeSimone, J. M.; Meyer, T. J. *Proc. Natl. Acad. Sci. U.S.A.* **2000**, *97*, 7687.
- (5) Meyer, T. J. *Acc. Chem. Res.* **1989**, *22*, 163.
- (6) Vos, J. G.; Kelly, J. M. *Dalton Trans.* **2006**, *41*, 4869.
- (7) Drummond, T. G.; Hill, M. G.; Barton, J. K. *Nat. Biotechnol.* **2003**, *21*, 1192.
- (8) Lainé, P. P.; Campagna, S.; Loiseau, F. *Coord. Chem. Rev.* **2008**, *252*, 2552.
- (9) Balzani, V.; Juris, A.; Venturi, M.; Campagna, S.; Serroni, S. *Chem. Rev.* **1996**, *96*, 759.
- (10) Campagna, S.; Puntoriero, F.; Nastasi, F.; Bergamini, G.; Balzani, V. *Top. Curr. Chem.* **2007**, *280*, 117.
- (11) Juris, A.; Balzani, V.; Barigelletti, F.; Campagna, S.; Belsler, P.; Von Zelewsky, A. *Coord. Chem. Rev.* **1988**, *84*, 85.
- (12) Friedman, A. E.; Chambon, J. C.; Sauvage, J. P.; Turro, N. J.; Barton, J. K. *J. Am. Chem. Soc.* **1990**, *112*, 4960.

- (13) Campagna, S.; Serroni, S.; Bodige, S.; MacDonnell, F. M. *Inorg. Chem.* **1999**, *38*, 692.
- (14) Hartshorn, R. M.; Barton, J. K. *J. Am. Chem. Soc.* **1992**, *114*, 5919.
- (15) Grover, N.; Neyhart, G. A.; Liang, W. G.; Singh, P.; Thorp, H. H. *Angew. Chem., Int. Ed. Engl.* **1992**, *31*, 1048.
- (16) Sun, Y.; Lutterman, D. A.; Turro, C. *Inorg. Chem.* **2008**, *47*, 6427.
- (17) Brown, W. R.; McGarvey, J. J. *Coord. Chem. Rev.* **2006**, *250*, 1696.
- (18) Batista, E. R.; Martin, R. L. *J. Phys. Chem. A* **2005**, *109*, 3128.
- (19) Olson, E. J. C.; Hu, D.; Hormann, A.; Jonkman, A. M.; Arkin, M. R.; Stemp, E. D. A.; Barton, J. K.; Barbara, P. F. *J. Am. Chem. Soc.* **1997**, *119*, 11458.
- (20) (a) Xu, L. C.; Li, J.; Shen, Y.; Zheng, K. C.; Ji, L. N. *J. Phys. Chem. A* **2007**, *111*, 273. (b) Li, J.; Chen, J. C.; Xu, L. C.; Zheng, K. C.; Ji, L. N. *J. Organomet. Chem.* **2007**, *692*, 831.
- (21) Coates, C. G.; Olofsson, J.; Coletti, M.; McGarvey, J. J.; Önfelt, B.; Lincoln, P.; Nordén, B.; Tuite, E.; Matousek, P.; Parker, A. W. *J. Phys. Chem. B* **2001**, *105*, 12653.
- (22) Lutterman, D. A.; Chouai, A.; Liu, Y.; Sun, Y.; Stewart, C. D.; Dunbar, K. R.; Turro, C. *J. Am. Chem. Soc.* **2008**, *130*, 1163.
- (23) (a) Önfelt, B.; Lincoln, P.; Nordén, B. *J. Am. Chem. Soc.* **2001**, *123*, 3630. (b) Önfelt, B.; Olofsson, J.; Lincoln, P.; Nordén, B. *J. Phys. Chem. A* **2003**, *107*, 1000. (c) Olofsson, J.; Önfelt, B.; Lincoln, P. *J. Phys. Chem. A* **2004**, *108*, 4391.

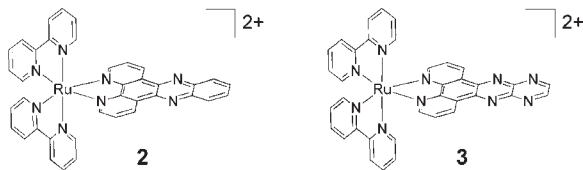


Figure 1. Molecular structures of **2** and **3**.

that its lowest-energy excited state is the nonemissive Ru \rightarrow dpdz $^3\text{MLCT}^{\text{dis}}$ state, whereas the luminescent $^3\text{MLCT}^{\text{prox}}$ state lies at a higher energy.^{23,24} The lack of luminescence from $^3\text{MLCT}^{\text{dis}}$ in **2** can be attributed to various factors, including the low energy of the excited state, resulting in increased nonradiative deactivation, and poor electronic coupling due to the longer donor/acceptor distance.^{22–24} The relative energies of the $^3\text{MLCT}^{\text{prox}}$ and $^3\text{MLCT}^{\text{dis}}$ states are highly dependent on the environment, and the light-switch effect can be explained by changes in the equilibrium, thus shifting the population between the emissive and nonemissive (or weakly emissive) states of **2** when bound to DNA or when free in solution.^{12,23,24} The luminescence of $[\text{Ru}(\text{bpy})_2\text{L}]^{2+}$ and $[\text{Ru}(\text{phen})_2\text{L}]^{2+}$ (phen = 1,10-phenanthroline), where L represents a dpdz derivative, such as dpdx (7,8-dimethyldipyridophenazine), dpdm2 (6-methyldipyridophenazine), tpphz (tetrapyrido[3,2-*a*:2',3'-*c*:3''-*c*:2'''-*h*:2''',3'''-*f*]phenazine), dpdp2 (pyrido[2',3':5,6]pyrazino[2,3-*f*][1,10]phenanthroline), and PHEHAT (1,10-phenanthroline[5,6-*b*]1,4,5,8,9,12-hexaazatriphenylene), has been reported to be very weak in water.^{14,16,25} The emission intensities of some of these complexes are enhanced upon the addition of DNA, but in general the magnitudes do not parallel those observed for **2**.^{14,16,25} It was reported that $[\text{Ru}(\text{TAP})_2(\text{dpdz})]^{2+}$ (TAP = 1,4,5,8-tetraazaphenanthrene) is highly emissive in water ($\Phi = 0.035$), however, in this complex, the lowest $^3\text{MLCT}$ state corresponds to a charge transfer from Ru^{II} to one of the two TAP ligands instead of dpdz.²⁶ In general, a similarity among heteroleptic $[\text{Ru}(\text{bpy})_2\text{L}]^{2+}$ (L = dpdz and its derivatives) complexes is their weak luminescence in aqueous media at room temperature.¹⁴

The present work focuses on a new member of the $[\text{Ru}(\text{bpy})_2\text{L}]^{2+}$ (L = dpdz and its derivatives) family of complexes, $[\text{Ru}(\text{bpy})_2(\text{dpqp})]^{2+}$ (**3**; dpqp = pyrazino[2',3':5,6]pyrazino[2,3-*f*][1,10]phenanthroline; Figure 1), which exhibits unusually strong luminescence in water at room temperature. This behavior is strikingly different from that of **2** and related complexes. The photophysical properties, electrochemistry, DNA binding, and DNA photocleavage of **3** were explored and compared to those of **2**, and electronic structure calculations were performed to aid in the interpretation of the results.

Experimental Section

Materials. The ligands 2,2'-bipyridine (bpy) and 1,10-phenanthroline (phen) and the precursor 2,3-diaminopyrazine were

purchased from Aldrich or Ark Pharm and used as received. Calf thymus DNA was purchased from Sigma and was dialyzed against 5 mM Tris buffer (50 mM NaCl, pH = 7.5) three times over a period of 48 h until $A_{260}/A_{280} > 1.8$, where A_{260} and A_{280} represent the absorbance at 260 and 280 nm, respectively.²⁷ $\text{Ru}(\text{bpy})_2\text{Cl}_2$,²⁸ 1,10-phenanthroline-5,6-dione,²⁹ $[\text{Ru}(\text{bpy})_3](\text{PF}_6)_2$,³⁰ and $[\text{Ru}(\text{bpy})_2(\text{dpdz})](\text{PF}_6)_2$ ¹⁶ were prepared according to literature methods.

dpqp. dpqp was synthesized according to a modified reported method,³¹ where 0.21 g of 1,10-phenanthroline-5,6-dione and 0.11 g of 2,3-diaminopyrazine were refluxed in 25 mL of CHCl_3 for 2 h. The solution was allowed to cool to room temperature and was kept in an ice bath overnight. The mixture was filtered, and the light-yellow solid was dried under vacuum. Yield: 0.25 g (88%). $^1\text{H NMR}$ (400 MHz, DMSO with 1 drop of D_2O): δ 8.65 (dd, $J = 4.61$ and 1.40 Hz, 2H), 8.19–8.07 (m, 2H), 7.44 (dd, $J = 7.65$ and 4.78 Hz, 2H), 7.28 (s, 2H). ESI MS: m/z 343.1 (dpqp \cdot 2H₂O + Na⁺). Anal. Calcd for $\text{C}_{16}\text{H}_8\text{N}_6 \cdot 4\text{H}_2\text{O}$: C, 53.93; H, 4.53; N, 23.58. Found: C, 54.28; H, 4.39; N, 23.22.

$[\text{Ru}(\text{bpy})_2(\text{dpqp})](\text{PF}_6)_2$, **[3](PF₆)₂**. $[\text{Ru}(\text{bpy})_2(\text{dpqp})](\text{PF}_6)_2$ was synthesized by the coordination of dpqp to $\text{Ru}(\text{bpy})_2\text{Cl}_2$ in EtOH/H₂O (1:1) in 73% yield.^{16,31} $^1\text{H NMR}$ (400 MHz, CD₃CN): δ 9.23 (dd, $J = 8.35$ and 1.30 Hz, 2H), 8.51 (dd, $J = 15.19$ and 8.04 Hz, 6H), 8.09 (dt, $J = 8.11$, 8.00, and 1.49 Hz, 2H), 7.99 (d, $J = 4.92$ Hz, 4H), 7.85 (d, $J = 5.54$ Hz, 2H), 7.78–7.70 (m, 2H), 7.59 (d, $J = 6.16$ Hz, 2H), 7.50–7.40 (m, 2H), 7.21 (dtd, $J = 6.88$, 5.61, 5.54, and 1.18 Hz, 2H). ESI MS: m/z 879.1 ($[\text{Ru}(\text{bpy})_2(\text{dpqp})](\text{PF}_6)_2 \cdot 2\text{H}_2\text{O}^+$). Anal. Calcd for $\text{C}_{36}\text{H}_{24}\text{F}_{12}\text{N}_{10}$: P₂Ru \cdot 3H₂O: C, 41.51; H, 2.90; N, 13.45. Found: C, 41.11; H, 2.60; N, 13.09.

Instrumentation. $^1\text{H NMR}$ spectra were collected on a 400 MHz Bruker system, and chemical shifts were referenced to the residual solvent peak. Electrochemical studies were carried out on a CV-50W voltammetric analyzer in a three-electrode cell with a glassy carbon working electrode, a platinum wire auxiliary electrode, and a saturated calomel electrode as the reference electrode. The measurements were conducted at a scan rate of 100 mV s⁻¹ in deoxygenated anhydrous CH₃CN containing 0.1 M tetra-*n*-butylammonium hexafluorophosphate as the supporting electrolyte. At the end of each experiment, a small amount of ferrocene (Fc) was added as an internal standard, and $E_{1/2}(\text{Fc}^{+/0}) = +0.66$ V vs normal hydrogen electrode (NHE) was used as the reference for calculation of the redox potential of each complex.¹⁶ Steady-state absorption spectra were recorded on a HP diode-array spectrometer (HP 8453) equipped with HP8453 WinSystem software. Corrected steady-state emission and excitation spectra were measured on a SPEX Fluoromax-2 spectrometer with a 90° optical geometry equipped with a 150 W xenon arc lamp as the source. The home-built transient absorption instrument for measurements on the nanosecond and microsecond time scales was previously described in detail.³² Excitation was accomplished through the use of a frequency-tripled (355 nm) Spectra-Physics GCR-150 Nd:YAG laser (fwhm \sim 8 ns). A 150 W xenon arc lamp in a PTI housing (Milliarc Compact Lamp Housing) powered by an LPS-220 power supply (PTI) with an LPS-221 igniter (PTI) was used as the irradiation source for the DNA photocleavage experiments. The irradiation wavelength was selected by placing long-pass colored glass filters (Melles Griot) between the source and the

(27) Marmur, J. *J. Mol. Biol.* **1961**, *3*, 208.

(28) Sullivan, B. P.; Salmon, D. J.; Meyer, T. J. *Inorg. Chem.* **1978**, *17*, 3334.

(29) (a) Bodge, S.; MacDonnell, F. M. *Tetrahedron Lett.* **1997**, *38*, 8159.

(b) Zhang, Z. B.; Yan, W. P.; Fan, M. G. *Chin. J. Appl. Chem.* **2005**, *22*, 103.

(30) Palmer, R. A.; Piper, T. S. *Inorg. Chem.* **1966**, *5*, 864.

(31) Bolger, J.; Gourdon, A.; Ishow, E.; Launay, J. P. *Inorg. Chem.* **1996**, *35*, 2937.

(32) Warren, J. T.; Chen, W.; Johnston, D. H.; Turro, C. *Inorg. Chem.* **1999**, *38*, 6187.

(24) (a) Brennaman, M. K.; Meyer, T. J.; Papanikolas, J. M. *J. Phys. Chem. A* **2004**, *108*, 9938. (b) Brennaman, M. K.; Alstrum-Acevedo, J. H.; Fleming, C. N.; Jang, P.; Meyer, T. J.; Papanikolas, J. M. *J. Am. Chem. Soc.* **2002**, *124*, 15094.

(25) Boisdenghien, A.; Moucheron, C.; Kirsch-De Mesmaeker, A. *Inorg. Chem.* **2005**, *44*, 7678.

(26) Ortmans, I.; Elias, B.; Kelly, J. M.; Moucheron, C.; Kirsch-DeMesmaeker, A. *Dalton Trans.* **2004**, 668.

Table 1. Photophysical Properties, Electrochemical Data, Sensitized Singlet Oxygen Quantum Yield, and Comparison to Calculations for 1–3

complex	$\lambda_{\text{abs}}/\text{nm}$ ($\epsilon \times 10^3/\text{M}^{-1}\text{cm}^{-1}$) ^a	$\lambda_{\text{em}}/\text{nm}$ (τ/ns)		I/I_0 ^b	$\lambda_{\text{em}}/\text{nm}$ ^c	Φ_{O_2} ^d	$E_{1/2}/\text{V}$ ^e	$\Delta E_{\text{exp}}^f/\text{V}$	$\Delta E_{\text{calc}}^g/\text{eV}$
		H ₂ O	CH ₃ CN						
1	287 (61.9), 450 (13.0)	626 (630)	619 (974)	~ 1.0 ^h	582, 629	0.81	1.52, -1.07, -1.26		
2	359 (17.5), 370 (17.2), 445 (16.3)	<i>i</i>	631 (750)	$> 10^4$ ^j	582, 630	0.16	1.57, -0.73, -1.15	0.34	0.33
3	365 (16.4), 430 (10.4), 457 (12.3)	617 (582)	618 (921)	1.1	576, 625	0.76	1.60, -0.33, ^k -1.08	0.74	0.76

^a H₂O. ^b Enhancement of the emission intensity of 1–3 upon the addition of calf thymus DNA in Tris buffer, [DNA]/[complex] = 10, [complex] = 10 μM . ^c At 77 K in EtOH/MeOH (4:1, v/v). ^d In CH₃OH. ^e In CH₃CN with 0.1 M Bu₄NPF₆, vs NHE. ^f $\Delta E_{\text{exp}} = E_{1/2}[\text{complex}]^{2+/+} - E_{1/2}[\text{1}]^{2+/+}$. ^g $\Delta E_{\text{calc}} = \text{LUMO}(\text{1}) - \text{LUMO}(\text{complex})$. ^h From ref 51. ⁱ Undetectable. ^j From ref 12. ^k Quasi-reversible.

sample. The ethidium bromide stained agarose gels were imaged using a GelDoc 2000 transilluminator (BioRad) equipped with Quantity One (version 4.0.3) software.

Methods. Photophysical measurements were performed in a long-neck, 1 × 1 cm quartz cuvette equipped with a rubber septum, and the solutions were bubbled with argon for ~10 min prior to each measurement, unless otherwise noted. Emission quantum yields were measured using [Ru(bpy)₃]²⁺ in deoxygenated CH₃CN ($\Phi = 0.062$) as the standard.³³ The binding constants of the metal complexes to DNA were determined by absorption titrations at room temperature with a ~10 μM metal complex and 0–75 μM calf-thymus DNA (ct-DNA; 5 mM Tris/HCl, 50 mM NaCl, pH = 7.5). The DNA binding constants, K_b , were obtained from fits of the titration data, as previously reported.³⁴ DNA photocleavage experiments were carried out using a 20 μL total sample volume in 0.5 mL transparent Eppendorf tubes containing 100 μM pUC18 plasmid and 20 μM of each ruthenium complex (5 mM Tris, pH = 7.4, 50 mM NaCl). The molecular and electronic structure calculations were performed with density functional theory (DFT) using the Gaussian03 (G03) program package. The B3LYP functional³⁵ with the 6-31G* basis set was used for hydrogen, carbon, and nitrogen³⁶ and the Stuttgart/Dresden (SDD) energy-consistent pseudopotentials for ruthenium.³⁷ The geometries of the ground states of 1–3 were optimized in acetonitrile using the conductive polarizable continuum model method with subsequent frequency analysis to show that the structures are at the local minima on the potential energy surface.³⁸ The electronic orbitals were visualized using GaussView 3.0.

Results and Discussion

Photophysical Properties and pH Dependence. The electronic absorption maxima, molar extinction coefficients, and emission properties of 1–3 are listed in Table 1. The absorption, excitation, and emission spectra of 3 at room temperature in water and at 77 K in MeOH/EtOH (1:4, v/v) are plotted in Figure 2. Complex 3 exhibits the typical singlet metal-to-ligand charge-transfer (¹MLCT) absorption band of ruthenium polypyridyl complexes with a maximum at 457 nm and a shoulder at ~430 nm (Figure 2 and Table 1).¹¹ In the ultraviolet region, its absorption is

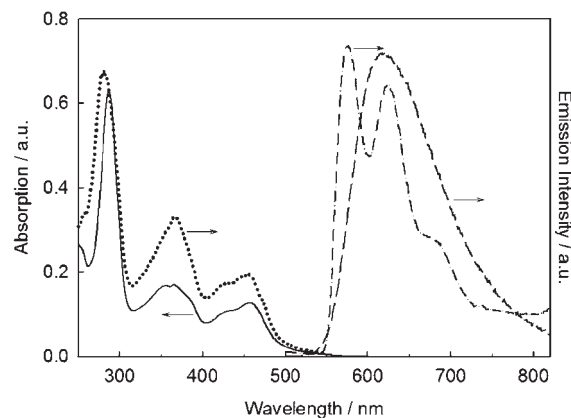


Figure 2. Electronic absorption (solid), excitation (dotted, $\lambda_{\text{em}} = 617$ nm), and emission spectra in water at 298 K (dashed line; $\lambda_{\text{exc}} = 450$ nm) and in EtOH/MeOH (4:1, v/v) at 77 K (dot-dashed line) of 3 (10 μM).

dominated by the intense ligand-centered (LC) $\pi\pi^*$ transition from the ancillary bpy ligands with a maximum at 287 nm.¹¹ A peak at 365 nm is attributed to the dpqp-based LC transition, a feature similar to those of 2 at 359 and 370 nm. However, unlike 2, which is not emissive in water, 3 exhibits strong luminescence ($\Phi_{\text{em}} = 0.039$) with a maximum at 617 nm that can be fitted to a monoexponential decay with $\tau = 582$ ns ($\lambda_{\text{exc}} = 355$ nm, fwhm ~8 ns, under argon; Figure 2). These values are comparable to those of 1 in water ($\Phi_{\text{em}} = 0.042$, $\lambda_{\text{em}} = 626$ nm, $\tau = 630$ ns). The excitation spectrum of 3 monitored at 617 nm overlaps well with its ground state absorption spectrum in water, indicating that the strong luminescence arises from 3 and not from a highly emissive impurity. As shown in Figure 2, the 77 K emission spectrum of 3 displays a vibronic structure with maxima at 576 and 625 nm ($\Delta\nu \approx 1361$ cm^{-1}) that is typical of the ³MLCT luminescence of ruthenium polypyridyl complexes, including 1 (582 and 629 nm; $\Delta\nu \approx 1284$ cm^{-1}) and 2 (582 and 630 nm; $\Delta\nu \approx 1309$ cm^{-1}) under similar experimental conditions (Table 1).¹¹

Figure 3 shows the transient absorption spectrum of 3 in CH₃CN, featuring a strong absorption band at 370 nm that is characteristic of the bpy radical anion in the ³MLCT state and bleaching of the ground state MLCT absorption in the 400–500 nm region ($\lambda_{\text{exc}} = 355$ nm; fwhm ~8 ns, under argon).³⁹ The signals at 450 and 370 nm can be fitted to monoexponential decays with lifetimes of 925 and 962 ns, respectively, which are similar to the luminescence lifetime of 3 in CH₃CN ($\tau = 921$ ns) with a

(33) Caspar, J. V.; Meyer, T. J. *J. Am. Chem. Soc.* **1983**, *105*, 5583.

(34) (a) Carter, M. T.; Rodriguez, M.; Bard, A. J. *J. Am. Chem. Soc.* **1989**, *111*, 8901. (b) Kalsbeck, W. A.; Thorp, H. H. *J. Am. Chem. Soc.* **1993**, *115*, 7146. (c) Chouai, A.; Wicke, S. E.; Turro, C.; Bacsá, J.; Dunbar, K. R.; Wang, D.; Thummel, R. P. *Inorg. Chem.* **2005**, *44*, 5996.

(35) (a) Becke, A. D. *Phys. Rev. A: Gen. Phys.* **1988**, *38*, 3098. (b) Becke, A. D. *J. Chem. Phys.* **1993**, *98*, 5648.

(36) Hehre, W. J.; Radom, L.; Schleyer, P. v. R.; Pople, J. A. *Ab Initio Molecular Orbital Theory*; John Wiley & Sons: New York, 1986.

(37) (a) Dolg, M.; Stoll, H.; Preuss, H. *Theor. Chim. Acta* **1993**, *85*, 441. (b) Wedig, U.; Dolg, M.; Stoll, H. *Quantum Chemistry: The Challenge of Transition Metals and Coordination Chemistry*; Springer: Dordrecht, The Netherlands, 1986.

(38) (a) Fantacci, S.; De Angelis, F.; Selloni, A. *J. Am. Chem. Soc.* **2003**, *125*, 4381. (b) Fantacci, S.; De Angelis, F.; Sgamellotti, A.; Re, N. *Chem. Phys. Lett.* **2004**, *396*, 43.

(39) Schanze, K. S.; Walters, K. A. In *Molecular and Supramolecular Photochemistry*; Ramamurthy, V., Schanze, K. S., Eds.; Marcel Dekker: New York, 1998; Vol. 2, pp 75–127.

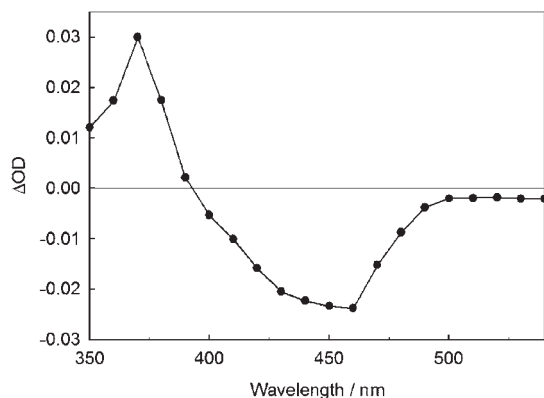


Figure 3. Transient absorption spectrum of **3** (60 μ M) in CH_3CN collected 20 ns after excitation ($\lambda = 355$ nm; fwhm ~ 8 ns).

maximum at 618 nm. These results indicate that both the transient absorption signal and the emission of the complex stem from the same excited state.³⁹ Together with the vibronic structure of the emission spectrum of **3** at 77 K, these results can be used to assign this excited state as ³MLCT.

The electronic absorption spectrum of **3** varies with the acidity of the solution, revealing the presence of two reversible protonation steps (Figure S1 in the Supporting Information). As shown in Figure S1a in the Supporting Information, when the volume of H_2SO_4 is increased from 0.2% to 24.2%, the intensity of the bpy-based LC transition decreases slightly and the dpqp $\pi\pi^*$ band red shifts and increases in intensity, with generation of an isosbestic point at 361 nm. A further increase from 24.2% to 64.6% H_2SO_4 results in the appearance of new features in the absorption spectrum of **3** along with a new isosbestic point at 395 nm (Figure S1b in the Supporting Information). In contrast, only one isosbestic point at 365 nm was observed for **2** up to 73.4% H_2SO_4 (Figure S2 in the Supporting Information), with no significant changes to the MLCT band of the complex. It should be noted that the absorption spectrum of **1** does not vary with pH under similar experimental conditions, consistent with previous reports.⁴⁰ The complete recovery of **3** from up to 64.4% H_2SO_4 can be achieved through the addition of NaOH, showing a remarkable stability of the complex in an acidic solution.

The red shift of the LC dpqp band from 365 to 417 nm with increasing H_2SO_4 can be interpreted as resulting from stabilization of the dpqp π^* orbitals upon protonation, as reported for other azaaromatic ligands.⁴¹ The stabilization is anticipated to make the protonated dpqp ligand easier to reduce, such that a red shift in the Ru \rightarrow dpqp MLCT transition is also expected. Although the position of the protonation of **3** cannot be ascertained, it is apparent that there are two protonation steps associated with dpqp. For **2**, protonation can only take place on the central (phenazine) portion of dpqz, and electronic repulsion makes a second protonation on the same ring unfavorable, although it may be possible under highly acidic conditions.⁴¹ Multiple protonation steps on the noncoordinated nitrogen atoms of azaaromatic ligands in

(40) Schilt, A. A. *J. Am. Chem. Soc.* **1963**, *85*, 904.

(41) Crutchley, R. J.; Kress, N.; Lever, A. B. P. *J. Am. Chem. Soc.* **1983**, *105*, 1170.

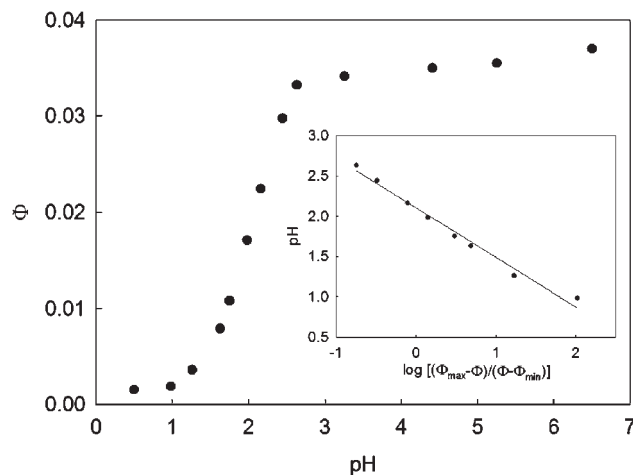


Figure 4. Variation of the quantum yield of **3** as a function of pH (inset: plot of pH vs $\log[(\Phi_{\text{max}} - \Phi)/(\Phi - \Phi_{\text{min}})]$ fitted to eq S1 in the Supporting Information).

acidic media have been reported for $[\text{Ru}(\text{bpz})_3]^{2+}$ (bpz = 2,2'-bipyrazine) and $[\text{Ru}(\text{bpm})_3]^{2+}$ (bpm = 2,2'-bipyrimidine).^{41,42}

The emission spectrum of **3** was also investigated as a function of solution pH. As shown in Figure 4, the luminescence quantum yield of **3** is relatively constant from pH = 6.8 to 2.6 ($\Phi = 0.035$ – 0.039) but decreases at pH < 2.6. The apparent excited state $\text{p}K_{\text{a}}^*$ value of **3** was calculated to be 2.1 from the changes in the luminescence intensity as a function of the pH fitted to eq S1 in the Supporting Information (inset of Figure 4).⁴³ Protonation of the excited states of other ruthenium complexes was investigated previously;^{41,42,44,45} for example, an apparent $\text{p}K_{\text{a}}^*$ of 2.0 was reported for the first protonation step of $[\text{Ru}(\text{bpz})_3]^{2+}$,⁴¹ and $\text{p}K_{\text{a}}^*$ values of 3.1–4.0 have been reported for the ruthenium complexes with bpy and TAP ligands.⁴⁴ Similarly, a series of 10 ruthenium complexes with the general formula $[\text{Ru}(\text{bpy})_3 - m - z(\text{bpm})_m - (\text{bpz})_z]^{2+}$ ($m, z = 0, 1, 2, 3; m + z \leq 3$) exhibit apparent $\text{p}K_{\text{a}}^*$ values in the range of 1.9–3.5, with the exception of $[\text{Ru}(\text{bpy})_3]^{2+}$.⁴²

Electrochemistry and Calculations. The oxidation and reduction potentials of **1–3** are listed in Table 1. Complex **3** possesses a reversible Ru^{III/II} oxidation wave at $E_{1/2}([\text{Ru}^{3+/2+}]) = +1.60$ V vs NHE, which appears at a slightly more positive potential typical of related ruthenium polypyridyl complexes.¹¹ A bpy-based reversible reduction potential of -1.08 V vs NHE is measured for **3**, similar to that of **1** at -1.07 V vs NHE. In addition, a quasi-reversible reduction potential centered on the dpqp ligand at -0.33 V vs NHE is observed for **3** and is also apparent in the free ligand (Figure S3 in the Supporting Information). Quasi-reversible reduction peaks have been reported for a similar ligand, dipyrido[3,2-*f*:2',3'-*h*]quinoxalino[2,3-*b*]quinoxaline.⁴⁶

(42) Sun, H.; Hoffman, M. Z. *J. Phys. Chem.* **1993**, *97*, 5014.

(43) Goncalves, H. M. R.; Maule, C. D.; Jorge, P. A. S.; Esteves da Silva, J. C. G. *Anal. Chim. Acta* **2008**, *626*, 62.

(44) (a) Kirsch-De Mesmaeker, A.; Jacquet, L.; Nasielski, J. *Inorg. Chem.* **1988**, *27*, 4451. (b) Herman, L.; Elias, B.; Pierard, F.; Moucheron, C.; Kirsch-DeMesmaeker, A. *J. Phys. Chem. A* **2007**, *111*, 9756.

(45) De Cola, L.; Prodi, L.; Zaccheroni, N.; König, B. *Inorg. Chim. Acta* **2002**, *336*, 1.

(46) da Silva Miranda, F.; Signori, A. M.; Vicente, J.; de Souza, B.; Priebe, J. P.; Szpoganicz, B.; Goncalves, N. S.; Neves, A. *Tetrahedron* **2008**, *64*, 5410.

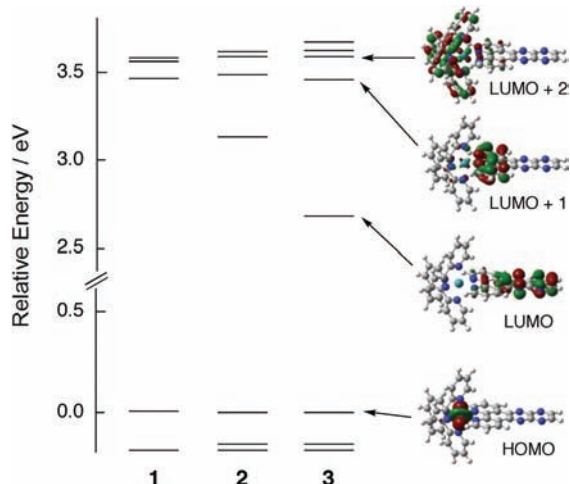


Figure 5. Energy diagram of the calculated MOs of **1–3**, with each HOMO set at 0 eV (isovalue = 0.04).

It is evident from a comparison of the data in Table 1 that dpqp is easier to reduce than dpbz and bpy.

DFT calculations were also performed to aid in the interpretation of the differences in the photophysical properties of **1–3**. Given the relative invariance of the oxidation potentials of **1–3** (Table 1), the highest occupied molecular orbitals (HOMOs) of **1–3** were set at 0 eV in the MO diagrams shown in Figure 5.¹⁶ For each complex, a set of three occupied molecular orbitals corresponding to ruthenium d orbitals were calculated (Table S1 in the Supporting Information), comprising HOMO, HOMO–1, and HOMO–2. The lowest unoccupied molecular orbital (LUMO) of **1** was calculated to possess bpy(π^*) character, consistent with previous reports,⁴⁷ whereas those of **2** and **3** were found to be localized on the distal portions of the dpbz and dpqp ligands, respectively. The LUMOs of **2** and **3** are calculated to lie at 0.33 and 0.76 eV lower energies than that of **1**, respectively (ΔE_{calc}). The values of ΔE_{calc} compare well with the experimental difference in the first reduction potentials of **2** and **3** relative to that of **1** (ΔE_{exp}), 0.34 and 0.74 V, respectively (Table 1). The agreement in the ΔE_{calc} and ΔE_{exp} values for each complex validates the calculated relative energies of the LUMOs of **1–3**. Selected calculated MOs of **3** are visualized in Figure 5, and the calculated MOs of **1** and **2** are shown in Table S1 in the Supporting Information.

It has been proposed that the lowest energy nonemissive state of **2** in water arises from an electronic transition from Ru^{II} to the phenazine portion of the dpbz ligand (MLCT^{dis}), whereas the emissive state is a result of charge transfer from the metal center to the proximal part of dpbz or the ancillary bpy ligands (MLCT^{prox}).^{23,24} Because of the related π -extended structure of dpbz and dpqp, we expect the electronic transitions of **3** from Ru^{II} to the distal portion of dpqp to be nonemissive or weakly emissive (MLCT^{dis}) and those states with transitions to the proximal part of dpqp or the ancillary bpy ligands to be strongly emissive (MLCT^{prox}). It is clear from Figure 5

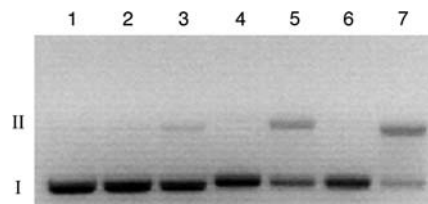


Figure 6. Ethidium bromide imaged agarose gel with 100 μM pUC18 plasmid and 20 μM chloride salt of each Ru^{II} complex in air (5 mM Tris, pH = 7.4, 50 mM NaCl): lane 1, plasmid only; lanes 2 and 3, **1**; lanes 4 and 5, **2**; lanes 6 and 7, **3**; lanes 1, 2, 4, and 6: dark; lanes 3, 5, and 7: $\lambda_{\text{irr}} \geq 455$ nm, $t_{\text{irr}} = 15$ min.

that the LUMO of **3**, which is localized on the distal portion of the ligand, lies at a significantly lower energy than that of **2**. Therefore, emission from $^3\text{MLCT}^{\text{dis}}$ in **3**, if detectable, would be expected to be observed at a significantly lower energy than that from $^3\text{MLCT}^{\text{prox}}$ in **2** and in **1**. However, the energy of the luminescence of **3** is nearly identical with that of **1** in water, with a vibronic structure at 77 K and transient absorption features similar to those of **1**. Although work is currently underway to further understand the photophysical properties of **3**, based on the current data collected at room temperature and in a glass matrix at 77 K, we propose that the emissive state of **3** is $^3\text{MLCT}^{\text{prox}}$, resulting from a transition from the metal center to the ancillary bpy ligands or the portion of the dpqp ligand proximal to the metal.

Interactions with DNA. The changes of the electronic absorption spectrum of **3** as a function of ct-DNA concentration were used to estimate the DNA binding constant, K_b (Figure S4 in the Supporting Information).³⁴ Hypochromic shifts were observed at 365 and 457 nm with a slight bathochromic shift (~ 2 nm) for 10.4 μM **3** in the presence of up to 71.5 μM ct-DNA, resulting in $K_b = 2.0 \times 10^6 \text{ M}^{-1}$ ($s = 1.62$) fitted as previously described in detail.³⁴ The DNA binding constant measured for **3** is similar to values reported for **2** (10^6 – 10^7 M^{-1}) and for related DNA intercalating complexes, with values that are several magnitudes greater than that of the nonintercalator **1** (700 M^{-1}).^{48–50} As listed in Table 1, only a modest (1.1-fold) luminescence enhancement is observed for 10 μM **3** upon the addition of 100 μM ct-DNA (5 mM Tris, 50 mM NaCl, pH = 7.5), a result that is strikingly different from that of the “light-switch” **2** under similar experimental conditions.¹² As previously reported, no observable luminescence changes in **1** were detected upon the addition of ct-DNA.⁵¹

The ethidium bromide stained agarose gel imaged in Figure 6 compares the DNA photocleavage of **1–3** upon irradiation ($\lambda_{\text{irr}} \geq 455$ nm, $t_{\text{irr}} = 15$ min). Lane 1 shows the migration of pUC18 alone kept in the dark as a control, which is composed mostly of unreacted supercoiled plasmid (form I). Without irradiation, no apparent DNA cleavage is observed in lanes 2, 4, and 6 for complexes **1–3**, respectively. Lanes 5 and 7 show the

(48) Pyle, A. M.; Rehmann, J. P.; Meshoyrer, R.; Kumar, C. V.; Turro, N. J.; Barton, J. K. *J. Am. Chem. Soc.* **1989**, *111*, 3051.

(49) Lincoln, P.; Broo, A.; Nordén, B. *J. Am. Chem. Soc.* **1996**, *118*, 2644.

(50) Erkkila, K. E.; Odom, D. T.; Barton, J. K. *Chem. Rev.* **1999**, *99*, 2777.

(51) Kumar, C. V.; Barton, J. K.; Turro, N. J. *J. Am. Chem. Soc.* **1985**, *107*, 5518.

(47) Nozaki, K.; Takamori, K.; Nakatsugawa, Y.; Ohno, T. *Inorg. Chem.* **2006**, *45*, 6161–6178.

DNA photocleavage of **2** and **3**, respectively, indicating greater reactivity of **3** compared to **2** under similar experimental conditions. This result is consistent with the greater quantum yield of the sensitized $^1\text{O}_2$ production of **3** ($\Phi_{^1\text{O}_2} = 0.76$) relative to that of **2** ($\Phi_{^1\text{O}_2} = 0.16$) measured in CH_3OH . Although **1** has a greater quantum yield for the production of $^1\text{O}_2$ (0.81), negligible DNA photocleavage is observed under similar conditions (lane 3). The difference in DNA photocleavage between **1** and **3** can be explained by the weak electrostatic DNA binding of the former and tight intercalation of the latter. The oxygen dependence of the DNA photocleavage by **3** was further investigated, and the results are shown in Figure S5 in the Supporting Information. Lanes 3 and 4 (Figure S5 in the Supporting Information) show greater DNA photocleavage by **3** in D_2O compared to H_2O , in agreement with the longer lifetime of $^1\text{O}_2$ in the former.⁵² Additionally, negligible DNA cleavage by **3** was observed under deoxygenated conditions (lane 5, Figure S5 in the Supporting Information). These findings suggest that the DNA photocleavage of **3** is primarily mediated by $^1\text{O}_2$.

(52) Rodgers, M. A. J.; Snowden, P. T. *J. Am. Chem. Soc.* **1982**, *104*, 5541.

Conclusions

In summary, a new ruthenium complex, **3**, that possesses a ligand related to dppz, dpqp, and exhibits unusually strong luminescence in aqueous media is reported. The pH dependence of the absorption spectra of **3** reveals two ground-state protonation steps associated with the dpqp ligand. Because of its strong DNA binding affinity and high quantum yield of sensitized $^1\text{O}_2$ production, complex **3** is able to cleave DNA more efficiently than **2** upon irradiation. The unusual photo-physical properties of **3** are believed to stem from a $^3\text{MLCT}$ excited state localized on the ancillary bpy ligands or the portion of the dpqp ligand proximal to the metal.

Acknowledgment. C.T. thanks the National Science Foundation (Grant CHE-0911354), The Ohio State University Institute for Materials Research and the Ohio Supercomputer Center. S.N.C. thanks James Aryeetey, Amelyne Major, Kristen Stoltz, and Roland Falcon for their contributions to this research effort.

Supporting Information Available: $\text{p}K_{\text{a}}^*$ determination, absorption changes as a function of the pH, cyclic voltammogram, calculated MOs of complexes **1**–**3**, DNA binding titration, and additional DNA photocleavage data. This material is available free of charge via the Internet at <http://pubs.acs.org>.